JACS
JOURNAL OF THE AMERICAN CHEMICAL SOCIETY

Communication

pubs.acs.org/JACS

Bioactive Polymeric Metallosomes Self-Assembled through Block Copolymer–Metal Complexation

Kensuke Osada,[†,∥] Horacio Cabral,[‡,∥] Yuki Mochida,[‡] Sangeun Lee,[‡] Kazuya Nagata,[§] Tetsuya Matsuura,[†] Megumi Yamamoto,[‡] Yasutaka Anraku,[†] Akihiro Kishimura,[†] Nobuhiro Nishiyama,[§] and Kazunori Kataoka*[,†,‡,§]

[†]Department of Materials Engineering and [‡]Department of Bioengineering, Graduate School of Engineering, The University of Tokyo, 7-3-1 Hongo, Bunkyo-ku, Tokyo 113-8656, Japan

[§]Division of Clinical Biotechnology, Center for Disease Biology and Integrative Medicine, Graduate School of Medicine, The University of Tokyo, 7-3-1 Hongo, Bunkyo-ku, Tokyo 113-8656, Japan

Supporting Information

ABSTRACT: Spontaneous formation of polymeric metallosomes with uniform size (~100 nm) was found to occur in aqueous medium through the reaction of an anticancer agent, (1,2-diaminocyclohexane)platinum(II) (DACHPt), with a Y-shaped block copolymer of ω-cholesteroyl-poly(L-glutamic acid) and two-armed poly(ethylene glycol) (PEGasus-PLGA-Chole). Circular dichroism spectrum measurements revealed that the PLGA segment forms an α-helix structure within the metallosomes, suggesting that secondary-structure formation of metallocomplexed PLGA segment may drive the self-assembly of the system into vesicular structure. These metallosomes can encapsulate water-soluble fluorescent macromolecules into their inner aqueous phase and eventually deliver them selectively into tumor tissues in mice, owing to the prolonged blood circulation. Accordingly, fluorescent imaging of the tumor was successfully demonstrated along with an appreciable antitumor activity by DACHPt moieties retained in the vesicular wall of the metallosomes, indicating the potential of metallosomes as multifunctional drug carriers.

Supramolecular architectures constructed through a self-assembly of block copolymers are attracting much interest because of their versatile morphologies. In particular, studies on vesicles (also known as polymersomes) have become a key area of focus because of interest in the study of their formation mechanisms,[1−4] morphology tuning,[5] and their potential as delivery carriers.[6] Various types of polymersomes have been developed from various interactions,[6] such as hydrophobic interactions by amphiphilic block copolymers, where the morphology can be modulated through ion−polymer complexation,[5,7] and electrostatic interactions from oppositely charged block copolymers.[8,9] The metal coordination bond is interesting as the membrane properties of polymersomes can be changed within water by a ligand-exchange reaction. This property is important for biomedical applications because the controlled release of loaded materials in the polymersomes is a crucial issue when the polymersomes are utilized as carriers to deliver therapeutic agents. Here, we succeeded to prepare spontaneous polymersome formation in water triggered by metal coordination bond, namely metallosomes, enabling the controlled release property of the cargos at the target site in the body. The metallosomes are formed between the aqueous complex of (1,2-diaminocyclohexane)platinum(II) (DACHPt), the active compound of the widely used platinum-based anticancer drug oxaliplatin,[10,11] and the carboxylic moieties of the poly(L-glutamic acid) (PLGA) segment of two-armed PEG-*b*-PLGA-cholesterol (PEGasus-PLGA-Chole), comprising the biocompatible components. The architecture of the metallosomes provides considerable storage capacity for water-soluble molecules within its inner water phase and, therefore, has tremendous potential for encapsulation and controlled delivery of water-soluble agents together with DACHPt moieties in the vesicular wall as anticancer agents. These metallosomes work as multifunctional drug carriers demonstrating tumor imaging through encapsulated fluorescent molecules within the inner aqueous phase along with appreciable antitumor activity.

The self-assembly occurred in water through complexation of DACHPt and PEGasus-PLGA-Chole block copolymers (PEGasus; 20 000 Da, degree of polymerization (DP) of PLGA; 20) (Figure 1a). A dynamic light scattering (DLS) measurement for this assembly showed a size of approximately 100 nm with narrow unimodal size distribution (Figure 1b). The structure of the assembly was investigated using transmission electron microscopy (TEM). The TEM image shown in Figure 1c was consistent with hollow vesicular structures, although collapse and aggregation occurred presumably during the vacuum treatment of the samples. Moreover, the vesicular assembly with clear thin membrane structure was observed in a cryogenic phase-contrast TEM (cryo-PCTEM) image (Figure 2a(i)), further supporting the formation of vesicles.

Given the vesicular nature of the assembly, it is possible to load hydrophilic molecules into its inner water space. Accordingly, PEGasus-PLGA-Chole and DACHPt were assembled in the presence of dextran labeled with FITC (FITC-dextran; 10 000 Da), and subsequently the solution was ultrafiltered to eliminate the FITC-dextran that was outside the assembly. The incorporation of the FITC-dextran into the

Received: May 11, 2012
Published: July 27, 2012

dx.doi.org/10.1021/ja304615y | J. Am. Chem. Soc. 2012, 134, 13172−13175

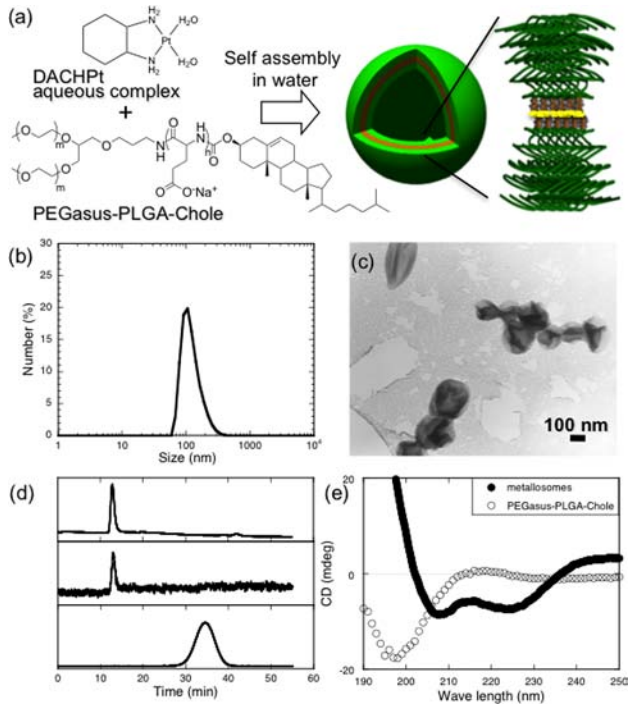

Figure 1. Formation and structure evaluations of metallosomes. (a) Schematic diagram of the proposed self-assembly of metallosomes through the formation of a metal complex between a Pt atom in the DACHPt and the carboxylic moiety of PLGA segment. (b) Size distribution of metallosomes measured by DLS. (c) Transmission electron micrograph of metallosomes stained with uranyl acetate. (d) Gel permeation chromatograms of FITC-dextran-loaded metallosomes (upper: UV absorption; center: fluorescence detection) and free FITC-dextran (lower: fluorescence detection). (e) CD spectra of metallosomes and PEGasus-PLGA-Chole block copolymer measured at neutral pH.

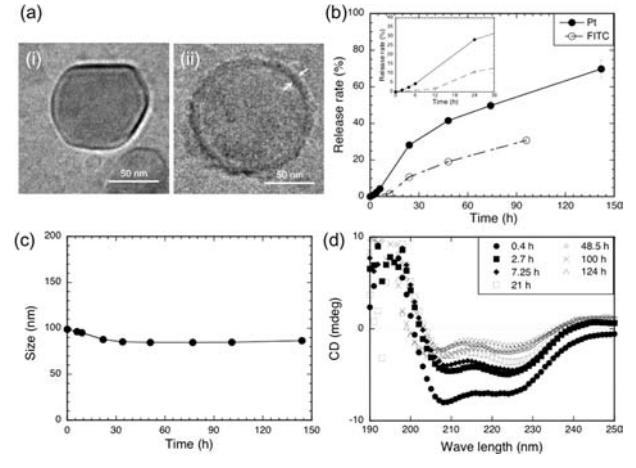

Figure 2. Release profiles of metallosomes under the physiological conditions (10 mM phosphate buffer (PB) plus 150 mM NaCl). (a) Cryogenic PCTEM images of metallosomes of (i) 0 h incubation and (ii) after 48 h incubation. Thickness of the vesicular membrane (indicated by arrows) was measured to be 6.3 nm in average from 11 independent metallosomes. (b) Release profiles of Pt complexes from the metallosomes and FITC-dextran from FITC-dextran-loaded metallosomes. Inset indicates the release profiles of early stage. Data are mean ± SD of $n = 3$. (c) Size change of metallosomes with incubation time determined by DLS. (d) Variation of CD spectra of the metallosomes with incubation time.

assembly was confirmed by gel permeation chromatography (GPC). The fluorescence of the incorporated FITC-dextran was determined at the same elution time as that of the assembly, whereas the free FITC-dextran appeared at a much later elution time (Figure 1d). This provided evidence for the coexistence of the FITC-dextran and the assembly. This result confirmed the vesicular nature of the assembly with inner water space; thus, it was named as "metallosome". Concurrently, the result indicates high potential of the metallosome as a reservoir for hydrophilic agents.

Formation of vesicular structures indicates that there may be particular structures of the constituent block copolymer that stabilize a lamellar phase of the vesicular membrane. Circular dichroism (CD) analysis revealed that the PLGA segment adopts an α-helix structure in metallosomes (Figure 1e, closed circle). PLGA is a well-known polypeptide that forms an α-helix under acidic conditions or when substituting side chains,[12] while adopting a random coil structure at neutral pH, as demonstrated by the CD spectrum of free PEGasus-PLGA-Chole block copolymer in the solution (Figure 1e, open circle). Binding of DACHPt to carboxylic moieties of PLGA induced α-helix formation even under neutral conditions, presumably because of decreased intramolecular electrostatic repulsion of the carboxylic moieties. Considering the inherent nature of cylindrical α-helices to pack laterally with each other[13−16] favoring formation of flat membrane and the nature of PEG and PLGA blocks to segregate, possible orientations of α-helices in the metallosome membrane are α-helices aligned (i) in an antiparallel manner to form a single layer or (ii) in a parallel manner to form double layers, with cholesterol (Chole) groups buried between the α-helix layers. From the viewpoint of free energy, the parallel alignment (ii) would be more favorable because hydrophobic Chole groups attached to the ω-end of the block copolymers can assemble between the α-helix double layers within a hydrophobic environment as schematically depicted in Figure 1a. Furthermore, Chole groups can assemble to form a cholesteric liquid crystal phase,[17,18] which could provide additional stability to the α-helix double layers. Moreover, well-controlled polymer segment lengths with narrow molecular weight distribution ($M_w/M_n = 1.05$) would facilitate interface alignment and lamellar formation. Assuming the parallel alignment as the most plausible structure, a molecular model calculated the double-layer thickness to be 7.0 nm [Supporting Information (SI)]. The measured thickness of the peripheral rings structure of the metallosome in cryo-PCTEM images (Figure 2a) was determined to be 6.3 nm ($n = 11$), which is comparable to the value calculated with the molecular model. Note that the PEG layer was not observed in the cryo-PCTEM images because of low electron density. The presence of Chole and PEGasus moieties in the block copolymers plays a crucial role for the vesicular formation because the combination of DACHPt and PEG-PLGA-Chole (no-branched linear PEG) resulted in polymeric micelles (Figure S1a, SI) and the combination of DACHPt and PEGasus-PLGA (without Chole) failed to form vesicles (Figure S1b, SI). As the metallosomes are formed in water, PLGA-Chole parts generate strong cohesive forces because of the presence of hydrophobic Chole groups and DACHPt molecules and, thus, tend to coagulate to decrease the interface to water. However, large osmotic pressure from the hydrated two-armed PEGasus tends to expand the interface. Under such frustrated conditions, the ordered alignment as lamellar may be favored to balance steric repulsion from the PEGasus layer and

dx.doi.org/10.1021/ja304615y | J. Am. Chem. Soc. 2012, 134, 13172−13175

coagulation of the α-helical cylinder with Chole moiety at ω-end.

The properties of metallosomes as drug carriers were then investigated. The amount of DACHPt in the metallosomes was determined by inductively coupled plasma-mass spectroscopy (ICP-MS) to be 10 wt % of the product. This is approximately 50% of the carboxylate moieties of PLGA complexed to DACHPt. The binding of DACHPt to PLGA is stable in distilled water but may be gradually cleaved under physiological NaCl conditions through the exchange reaction between chloride ions in the medium and the carboxylate group of the PLGA.[19] Thus metallosomes release the active Pt complexes in a sustained manner, achieving a discharge of more than 50% of the DACHPt after 72 h (Figure 2b inset). In contrast, a clear induction period during the first 12 h was observed in the release profile of Alexa 680-dextran (10 000 Da) incorporated in the interior of the metallosomes (Figure 2b). Presumably, the membrane of metallosomes is still not permeable to Alexa 680-dextran in the early stage until the release of a critical amount of Pt complex. This results in an increase in the threshold molecular weight cutoff of the membrane permeability, and ultimately enabling Alexa 680-dextran to penetrate the membrane. The initial induction phase is apparently an advantage when targeting solid tumors, as the release of the cargo in the inner phase is expected to occur after the vesicles reach the tumor tissue. Moreover, the induction period in dextran release suggests that the vesicular structure is assumed to be stable even after the substantial release of the Pt complex. Indeed the observation of the constant size of approximately 80 to 90 nm diameter for a prolonged time period at physiological NaCl concentration (Figure 2c) is consistent with the maintenance of the vesicular structure. Furthermore, the cryo-PCTEM images of the metallosomes incubated 48 h under physiological conditions revealed the presence of the vesicular structure (Figure 2a(ii)). CD intensity for the α-helix decreased with incubation time in physiological conditions (Figure 2d), indicating that the PLGA segments in the metallosome gradually underwent a transition from α-helix to random coil with the release of DACHPt. Yet, worthy to note is that the characteristic α-helix spectra still remained even after prolonged incubation, suggesting a crucial role of α-helices in maintaining the vesicular structure.

The small size of approximately 100 nm with PEGylated palisade of the metallosomes is a substantial advantage to attain prolonged blood circulation and ultimately increases the accumulation of metallosomes in tumors through passive targeting based on the EPR effect.[20] Moreover, metallosomes might be very valuable for the systemic codelivery of both the Pt complex and encapsulated agents in the hollow water space. Thus, blood circulation of the FITC-dextran-loaded metallosomes was evaluated through the detection of both Pt (Figure 3a) and FITC fluorescence (Figure 3b). The results clearly exhibited prolonged retention in the bloodstream for both species. Alternatively, both free oxaliplatin, which is an oxalate complex of DACHPt (Figure 3a), and free FITC-dextran (Figure 3b) were rapidly cleared from the bloodstream. Co-injection of free FITC-dextran with empty metallosomes revealed no improved plasma retention compared to the single injection (Figure 3b), excluding the possibility that the FITC-dextran adsorption to the metallosome surface brought the longevity in blood circulation. Eventually, the augmented bioavailability of metallosomes and the EPR effect enabled an increased accumulation of both DACHPt and FITC-dextran

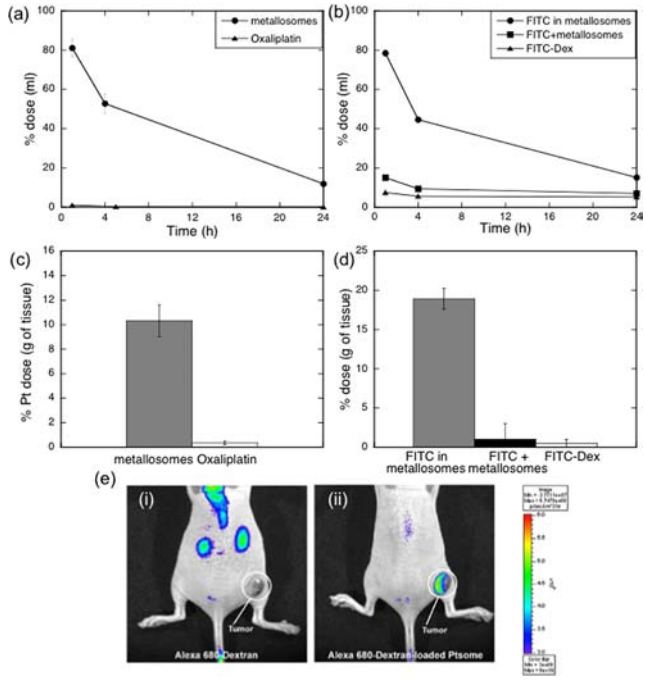

Figure 3. *In vivo* performance of metallosomes through i.v. injection. (a) Plasma clearance of Pt after injection of oxaliplatin and metallosomes. (b) Plasma clearance of free FITC-dextran, free FITC-dextran coinjected with metallosomes, and FITC-dextran-loaded metallosomes. (c) Tumor accumulation of Pt 24 h after injection for metallosomes and oxaliplatin. (d) Tumor accumulation of FITC-dextran 24 h after injection for FITC-dextran-loaded metallosomes, free FITC-dextran co-injected with metallosomes, and free FITC-dextran. (e) *In vivo* fluorescent imaging of free Alexa 680-dextran (i) and Alexa 680-dextran-loaded metallosomes (ii) 24 h after injection. Data are mean ± SD of $n = 6$.

into subcutaneous colon adenocarcinoma 26 (C26) tumors (Figure 3c,d), confirming the high potency of the metallosomes as the systemic multifunctional carrier.

In vivo noninvasive imaging of nanocarriers is plausible for determining their tissue selectivity and estimating their therapeutic and diagnostic potentials. In this regard, the preferential tumor accumulation of Alexa 680-dextran was clearly observed by *in vivo* near-infrared fluorescence imaging after the injection of Alexa 680-dextran-loaded metallosomes (Figure 3e). In contrast, the signal of Alexa 680-dextran injected in the free form mainly appeared at the kidneys, visually confirming the high capacity of metallosome as the nanocarrier directing encapsulated substances to solid tumors.

This elevated tumor accumulation of metallosomes is expected to improve the antitumor activity of the incorporated platinum drug, since DACHPt complexes can exert their cytotoxicity after being released from the metallosomes as observed in *in vitro* studies (Table S1, SI). We studied the antitumor activity of oxaliplatin and the metallosomes in C-26-bearing mice through intravenous (i.v.) injection. For free oxaliplatin, no inhibition of the tumor growth was observed at any dose in this condition (Figure 4a). Moreover, the mice injected with 10 mg/kg of oxaliplatin presented toxic death after the third injection (Figure 4b). Mice treated with 6 mg/kg of metallosomes achieved considerable reduction in the tumor growth rate ($p < 0.005$ at day 14) (Figure 4a), which was comparable to the previously reported data obtained for the DACHPt loaded micelles undergoing clinical trial,[21] because of

dx.doi.org/10.1021/ja304615y | J. Am. Chem. Soc. 2012, 134, 13172−13175

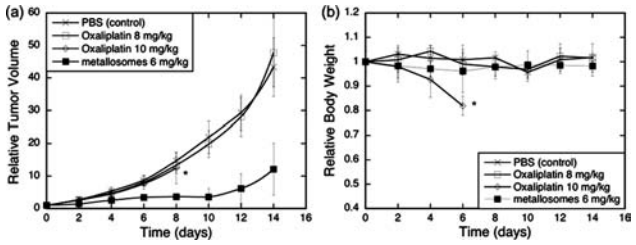

Figure 4. Antitumor activity of metallosomes through i.v. injection. (a) Relative tumor volume. (b) Relative body weight: oxaliplatin at 8 and 10 mg/kg and metallosomes at 6 mg/kg. Day 0 is the first day of injection. *Toxic death 6/6 mice. Data are mean ± SD of $n = 6$.

the high accumulation of drug in the tumor tissue without showing significant body weight loss (Figure 4b). The ability of metallosomes to load and deliver multiple therapeutic agents presents enormous possibilities for the design of new therapeutic strategies, such as loading different chemotherapeutic agents for improved combination chemotherapy or diagnosis agents for real-time monitoring of the therapeutic response.

The simple construction of metallosomes in water without use of organic solvents allows encapsulation of fragile bioactive compounds, and the observed *in vitro* and *in vivo* performance of the metallosomes against cancer offers a promising platform for the development of nanocarriers for versatile application. The tunable multifunctionality of block copolymers and the use of diverse metal coordination bond to assemble the vesicles will provide a method for creating smart carriers enabling both diagnosis and therapy, thereby reducing the complexity of multidrug administration.

■ ASSOCIATED CONTENT

Ⓢ Supporting Information

Materials and methods, TEM images of the assemblies prepared from PEG-PLGA-Chole or PEGasus-PLGA and DACHPt, molecular modeling of DACHPt/PLGA, and an additional table summarizing the *in vitro* cytotoxicity results. This material is available free of charge via the Internet at http://pubs.acs.org.

■ AUTHOR INFORMATION

Corresponding Author

kataoka@bmw.t.u-tokyo.ac.jp

Author Contributions

‖These authors contributed equally.

Notes

The authors declare no competing financial interest.

■ ACKNOWLEDGMENTS

This research was partly supported by Grant-in-Aid for Scientific Research on Priority Area "Cancer" from The Ministry of Education, Culture, Sports, Science and Technology, Japan, and by the Japan Society for the Promotion of Science (JSPS) through its "Funding Program for World-Leading Innovative R&D on Science and Technology (FIRST Program)."

■ REFERENCES

(1) Luo, L. B.; Eisenberg, A. *J. Am. Chem. Soc.* **2001**, *123*, 1012.
(2) Discher, D. E.; Eisenberg, A. *Science* **2002**, *297*, 967.
(3) Antonietti, M.; Forster, S. *Adv. Mater.* **2003**, *15*, 1323.
(4) Azzam, T.; Eisenberg, A. *Angew. Chem., Int. Ed.* **2006**, *45*, 7443.
(5) Christian, D. A.; Tian, A. W.; Ellenbroek, W. G.; Levental, I.; Rajagopal, K.; Janmey, P. A.; Liu, A. J.; Baumgart, T.; Discher, D. E. *Nat. Mater.* **2009**, *8*, 843.
(6) Meng, F. H.; Zhong, Z. Y.; Feijen, J. *Biomacromolecules* **2009**, *10*, 197.
(7) Zhang, L. F.; Yu, K.; Eisenberg, A. *Science* **1996**, *272*, 1777.
(8) Koide, A.; Kishimura, A.; Osada, K.; Jang, W. D.; Yamasaki, Y.; Kataoka, K. *J. Am. Chem. Soc.* **2006**, *128*, 5988.
(9) Anraku, Y.; Kishimura, A.; Oba, M.; Yamasaki, Y.; Kataoka, K. *J. Am. Chem. Soc.* **2010**, *132*, 1631.
(10) Kidani, Y.; Inagaki, K.; Iigo, M.; Hoshi, A.; Kuretani, K. *J. Med. Chem.* **1978**, *21*, 1315.
(11) Ibrahim, A.; Hirschfeld, S.; Cohen, M. H.; Griebel, D. J.; Williams, G. A.; Pazdur, R. *Oncologist* **2004**, *9*, 8.
(12) Nagasawa, M.; Holtzer, A. *J. Am. Chem. Soc.* **1964**, *86*, 538.
(13) Flory, P. J. *Proc. R. Soc. London, Ser. A* **1956**, *234*, 73.
(14) Parry, D. A.; Elliott, A. *Nature* **1965**, *206*, 616.
(15) Bellomo, E. G.; Wyrsta, M. D.; Pakstis, L.; Pochan, D. J.; Deming, T. J. *Nat. Mater.* **2004**, *3*, 244.
(16) Rodriguez-Hernandez, J.; Lecommandoux, S. *J. Am. Chem. Soc.* **2005**, *127*, 2026.
(17) Goodby, J. W. *Liq. Cryst.* **1998**, *24*, 25.
(18) Klok, H. A.; Hwang, J. J.; Iyer, S. N.; Stupp, S. I. *Macromolecules* **2002**, *35*, 746.
(19) Nishiyama, N.; Yokoyama, M.; Aoyagi, T.; Okano, T.; Sakurai, Y.; Kataoka, K. *Langmuir* **1999**, *15*, 377.
(20) Matsumura, Y.; Maeda, H. *Cancer Res.* **1986**, *46*, 6387.
(21) Cabral, H.; Nishiyama, N.; Kataoka, K. *J. Controlled Release* **2007**, *121*, 146.